

## Accepted Manuscript

Fading regularization MFS algorithm for the Cauchy problem associated with the two-dimensional Helmholtz equation

Laëtitia Caillé, Franck Delvare, Liviu Marin,  
Nathalie Michaux-Leblond

PII: S0020-7683(17)30328-1  
DOI: [10.1016/j.ijsolstr.2017.07.011](https://doi.org/10.1016/j.ijsolstr.2017.07.011)  
Reference: SAS 9657



To appear in: *International Journal of Solids and Structures*

Received date: 25 March 2017  
Revised date: 19 June 2017  
Accepted date: 7 July 2017

Please cite this article as: Laëtitia Caillé, Franck Delvare, Liviu Marin, Nathalie Michaux-Leblond, Fading regularization MFS algorithm for the Cauchy problem associated with the two-dimensional Helmholtz equation , *International Journal of Solids and Structures* (2017), doi: [10.1016/j.ijsolstr.2017.07.011](https://doi.org/10.1016/j.ijsolstr.2017.07.011)

This is a PDF file of an unedited manuscript that has been accepted for publication. As a service to our customers we are providing this early version of the manuscript. The manuscript will undergo copyediting, typesetting, and review of the resulting proof before it is published in its final form. Please note that during the production process errors may be discovered which could affect the content, and all legal disclaimers that apply to the journal pertain.

# FADING REGULARIZATION MFS ALGORITHM FOR THE CAUCHY PROBLEM ASSOCIATED WITH THE TWO-DIMENSIONAL HELMHOLTZ EQUATION

Laëtitia Caillé<sup>1,2,3,\*</sup>, Franck Delvare<sup>1,2,3,†</sup>, Liviu Marin<sup>4,5,‡</sup> and Nathalie Michaux-Leblond<sup>1,2,3,§</sup>

<sup>1</sup>Normandie Univ, <sup>2</sup>UNICAEN, LMNO, F-14032 Caen, France, <sup>3</sup>CNRS, UMR 6139, F-14032 Caen, France

<sup>4</sup>Department of Mathematics, Faculty of Mathematics and Computer Science, University of Bucharest, 14  
Academiei, 010014 Bucharest, Romania

<sup>5</sup>Institute of Mathematical Statistics and Applied Mathematics, Romanian Academy, 13 Calea 13 Septembrie,  
050711 Bucharest, Romania

## Abstract

In this paper, we combine the fading regularization method with the method of fundamental solutions (MFS) and investigate its application to the Cauchy problem for the two-dimensional Helmholtz equation. We present a numerical reconstruction of the missing data on an inaccessible part of the boundary from the knowledge of overprescribed noisy data taken on the remaining accessible boundary part for both smooth and piecewise smooth two-dimensional geometries. The accuracy, convergence, stability and efficiency of the proposed numerical algorithm, as well as its capability to deblur the noisy data, are validated by three numerical examples.

## 1 Introduction

The Helmholtz equation arises naturally in numerous physical and engineering applications such as the wave propagation and vibration phenomena. It is often used to describe the vibration of a structure [1],

---

\*E-mail: laetitia.caille@unicaen.fr

†Corresponding author. E-mail: franck.delvare@unicaen.fr

‡E-mails: marin.liviu@gmail.com; liviu.marin@fmi.unibuc.ro

§E-mail: nathalie.leblond@unicaen.fr

the acoustic cavity problem [2], the radiation wave [3] and the scattering of a wave [4]. The knowledge of Dirichlet, Neumann or mixed boundary conditions on the entire boundary of the domain leads to the so-called direct problems for the Helmholtz equation which have been extensively studied in the literature, see e.g. [5–7]. However, the boundary conditions available are often incomplete, either in the form of underspecified or overspecified boundary conditions on different parts of the boundary or the solution is prescribed at some internal points in the domain. These are referred to as inverse problems and it is well-known that they are generally ill-posed in the sense of Hadamard [8], i.e. the existence, uniqueness and stability of their solutions are not always guaranteed.

A classical example of an inverse problem for the Helmholtz equation is represented by the Cauchy problem, for which boundary conditions for both the solution and its normal derivative are prescribed only on a part of the boundary of the domain, whereas no information is available on the remaining boundary. Unlike direct problems, the uniqueness of the solution of the Cauchy problem is guaranteed if the boundary conditions are compatible, without the necessity of removing the eigenvalues of the Laplacian [9]. A BEM-based acoustic holography technique using the singular value decomposition (SVD) for the reconstruction of sound fields generated by irregularly shaped sources has been developed by Bai [10]. The vibrational velocity, sound pressure and acoustic power on the vibrating boundary comprising an enclosed space have been reconstructed by Kim and Ih [11], who have used the SVD to obtain the inverse solution in the least-squares sense and express the acoustic modal expansion between the measurement and source field. Wang and Wu [12] have developed a method using the spherical wave expansion theory and a least-squares minimisation to reconstruct the acoustic pressure field from a vibrating object. Their method has been extended to the reconstruction of acoustic pressure fields inside the cavity of a vibrating object by Wu and Yu [13]. DeLillo et al. [14] have detected the source of acoustical noise inside the cabin of a midsize aircraft from measurements of the acoustical pressure field inside the cabin by solving a linear Fredholm integral equation of the first kind. Iterative algorithms, such as an alternating iterative algorithm, the conjugate gradient method (CGM), the Landweber-Fridman iterative procedure and the minimal error method, have been used in conjunction

with the boundary element method (BEM) to solve in a stable manner the Cauchy problem for the two-dimensional Helmholtz equation, see e.g. [15–18]. The Tikhonov regularization method and the meshless method of fundamental solutions (MFS) have been combined in order to resolve the same inverse Cauchy problem in two [19] and three dimensions [20], respectively, whilst Jin and Marin [21] proposed the use of the plane wave method and the truncated singular value decomposition. The application of the Tikhonov functional and the dual reciprocity BEM (DRBEM) to the Cauchy problem for Helmholtz-type equations with variable coefficients was investigated by Marin et al. [22]. Qin et al. [23] reduced the Cauchy problem for the Helmholtz equation to a moment problem and, at the same time, provided an error estimate and its convergence analysis, whilst a truncation method, as well as convergence and stability results for a suitable choice of the regularization parameter, were addressed by Qin and Wei [24]. Kabanikhin et al. [25] introduced a gradient based algorithm applied to the continuation problem for the Cauchy problem associated with the Helmholtz equation and the singular value expansion of the operator corresponding to this continuation problem. Berntsson et al. [26] proposed and implemented an alternating iterative method for solving the Cauchy problem for the Helmholtz equation in a Lipschitz domain, whilst the same authors introduced and accelerated numerical solution of this inverse problem based on CGMs [27].

Cimetière et al. [28, 29] introduced the so-called fading regularization method to solve the Cauchy problem associated with the Laplace equation. This regularization procedure consists of an iterative process, whose convergence was also established, see Cimetière et al. [28, 29]. This approach reduces the resolution of the Cauchy problem to that of a sequence of optimization problems subject to an equality constraint. At each step of this iterative procedure, we look, among all solutions of the equilibrium equation, for those that approach at best the overspecified data and the previously computed optimal element. This is the reason why the functional to be minimized in the space that characterizes the solutions of the equilibrium equation, consists of two terms: a relaxation term which allows us to minimize the gap between the optimal element and the overspecified boundary data, and a regularization term which controls the gap between the actual optimal element and the previous one. In the case of

compatible data, it was also proved that the sequence converges to the solution of the given Cauchy problem. The additional regularization term tends to zero as the iterative procedure is continued and this is the reason why the method is referred to as the fading regularization method.

The fading regularization method was numerically implemented, in the case of the Cauchy problem for the Laplace operator, using both the BEM and the FEM by Delvare et al. [30] and Cimetière et al. [31], respectively, and it was later extended to solve Cauchy problems in two-dimensional elasticity in conjunction with the BEM [32], the FEM [33, 34] and the method of fundamental solutions (MFS) [35].

The MFS was originally proposed by Kupradze and Aleksidze [36] and since its introduction as a numerical method by Mathon and Johnston [37], it has been successfully applied to a large variety of direct and inverse problems in science and engineering [38–40]. The MFS is a meshless boundary collocation method which belongs to the family of so-called Trefftz methods, may be regarded as an approximation of the indirect BEM [41] and is relevant to boundary value problems for which a fundamental solution of the operator is known. In spite of the aforementioned restriction, the MFS is especially used because of the ease with which it can be implemented and its low computational cost.

The aim of this paper is to emphasize and combine the features of the fading regularizing algorithm and the MFS in order to obtain a robust, versatile, accurate, stable and convergent iterative procedure for the numerical solution of the Cauchy problem associated with the two-dimensional Helmholtz equation. The paper is organized as follows. In Section 2 we present the inverse problem under investigation. The fading regularization algorithm and the numerical method used for the approximate solution of the Cauchy problem, namely the MFS, are described in Sections 3.1 and 3.3, respectively. Three numerical examples related to simply and doubly connected two-dimensional geometries with a (piecewise) smooth boundary are considered and thoroughly investigated in Section 4. Finally, some concluding remarks and ideas for future work are presented in Section 5.

## 2 The Cauchy problem for the Helmholtz equation

Consider an open bounded domain  $\Omega \subset \mathbb{R}^2$  which is bounded by a piecewise smooth boundary  $\Gamma \equiv \partial\Omega$ , such that  $\Gamma = \Gamma_d \cup \Gamma_u$ , where  $\Gamma_d, \Gamma_u \neq \emptyset$  and  $\Gamma_d \cap \Gamma_u = \emptyset$ . We assume that  $u$  satisfies the Helmholtz equation in the domain  $\Omega$ , namely

$$(\Delta + k^2)u(\underline{x}) = 0, \quad \underline{x} \in \Omega, \quad (1)$$

where  $k^2 \in \mathbb{R}_+^*$ . Let  $\underline{n}(\underline{x})$  be the outward unit normal vector at a point  $\underline{x} \in \Gamma$  and  $\Phi(\underline{x}) = (\nabla u \cdot \underline{n})(\underline{x})$  be the flux at  $\underline{x} \in \Gamma$ .

If both the solution and its normal derivative can be measured on  $\Gamma_d$ , then this leads to the mathematical formulation of a Cauchy problem consisting of Eq. (1) and the boundary conditions

$$u(\underline{x}) = u_d(\underline{x}), \quad \Phi(\underline{x}) = \Phi_d(\underline{x}), \quad \underline{x} \in \Gamma_d, \quad (2)$$

where  $u_d$  and  $\Phi_d$  are prescribed functions on  $\Gamma_d \subset \Gamma$  and  $\text{meas}(\Gamma_d) > 0$ . In the above formulation of the boundary conditions (2), it can be seen that the boundary  $\Gamma_d$  is overspecified by prescribing both the solution  $u$  and its normal derivative  $\Phi$ , whilst the boundary  $\Gamma_u$  is underspecified since both the solution  $u$  and its normal derivative  $\Phi$  are unknown and have to be determined.

This problem, referred to as the Cauchy problem, is much more difficult to solve than the direct problem since its solution does not satisfy the general conditions of well-posedness. Whilst the Dirichlet, Neumann or mixed direct problems associated with Eq. (1) do not always have a unique solution due to the eigensolutions of the Laplacian [42], the solution of the Cauchy problem (1) and (2) is unique if it exists, based on the analytical continuation property [9]. However, it is well-known that if this solution exists, then it is unstable with respect to small perturbations in the data on  $\Gamma_d$  [8]. Thus, the problem under investigation is ill-posed and one cannot use a direct approach, such as the Gauss elimination method, in order to solve the system of linear equations which arises from the discretisation of (1) and (2). Therefore, regularization methods are required in order to solve accurately the Cauchy problem associated with the two-dimensional Helmholtz equation.

### 3 Fading regularization method

#### 3.1 Continuous formulation

We introduce the space  $H(\Omega)$  of solutions of equation (1) by

$$H(\Omega) = \{v \in H^1(\Omega) \mid v \text{ satisfies (1) in a weak sense} \},$$

This space is a closed subspace of  $H^1(\Omega)$  and hence a Hilbert space when equipped with the  $H^1(\Omega)$  scalar product. We further denote by  $H(\Gamma)$  the space of restrictions to  $\Gamma$  of elements  $v \in H(\Omega)$  and their corresponding normal derivatives  $v'$ , namely

$$H(\Gamma) = \left\{ \underline{U} = (u, u') \in H^{1/2}(\Gamma) \times H^{-1/2}(\Gamma) \mid \exists v \in H(\Omega) \text{ such that } v|_{\Gamma} = u \text{ and } v' = u' \right\}. \quad (3)$$

It can be easily shown that the space of compatible data  $H(\Gamma)$  is a closed subspace of  $H^{1/2}(\Gamma) \times H^{-1/2}(\Gamma)$  and it is, therefore, a Hilbert space when equipped with the scalar product

$$\langle \underline{U}, \underline{V} \rangle_{\Gamma} = \langle u, v \rangle_{\frac{1}{2}, \Gamma} + \langle u', v' \rangle_{-\frac{1}{2}, \Gamma}, \quad \forall \underline{U} = (u, u'), \underline{V} = (v, v') \in H(\Gamma). \quad (4)$$

The norm induced by this scalar product is denoted by  $\| \cdot \|_{\Gamma}$ .

Analogous to [28], we introduce the space  $H(\Gamma_d)$  of restrictions to  $\Gamma_d$  of elements from  $H(\Gamma)$ . Note that  $H(\Gamma_d)$  is a subspace of  $H^{\frac{1}{2}}(\Gamma_d) \times H^{-\frac{1}{2}}(\Gamma_d)$  and the norm induced on  $H(\Gamma_d)$  is denoted by  $\| \cdot \|_{\Gamma_d}$ .

An equivalent formulation of problem (1) and (2) reads as

$$\text{Find } \underline{U} = (u, \Phi) \in H(\Gamma) \text{ such that } \underline{U} = \underline{\psi}_d \text{ on } \Gamma_d, \quad (5)$$

where  $\underline{\psi}_d = (u_d, \Phi_d)$ .

Problem (5) is also ill-posed even if it admits a unique solution and hence an iterative regularizing method has to be introduced to solve it in a stable manner. This method is a generalization of the inverse technique introduced by Cimetière et al [28, 29] to solve the Cauchy problem for the Laplace equation and can be considered as an iterative Tikhonov-type method. Given  $c > 0$  and  $\underline{U}^0 \in H(\Gamma)$ ,

the iterative algorithm is given by

$$\begin{cases} \text{Find } \underline{U}^{k+1} \in H(\Gamma) \text{ such that} \\ J_c^k(\underline{U}^{k+1}) \leq J_c^k(\underline{V}) \quad \forall \underline{V} \in H(\Gamma) \text{ with} \\ J_c^k(\underline{V}) = \|\underline{V}|_{\Gamma_d} - \underline{\psi}_d\|_{\Gamma_d}^2 + c \|\underline{V} - \underline{U}^k\|_{\Gamma}^2. \end{cases} \quad (6)$$

In this iterative process, Eq. (1) is taken into account exactly since at each step of this procedure the search for an optimal element is performed in  $H(\Gamma)$ . The functional in (6) is composed of two terms which play different roles. The first one acts only on  $\Gamma_d$  and represents the gap between the optimal element and the overspecified boundary data. It relaxes the overspecified data which can be possibly perturbed by noisy measurements (i.e. a relaxation term). The second term in (6) acts on the entire boundary  $\Gamma$  and not only on  $\Gamma_u$ , where the boundary conditions are to be completed. This term is a regularization term and controls the distance between the new optimal element and the previous one and tends to zero as the number of iterations increases. Therefore, at each step of the iterative procedure, the optimal element obtained is an exact solution of Eq. (1) and is close to the overspecified data  $\underline{\psi}_d = (u^d, \Phi^d)$ . This unique optimal element  $\underline{U}^{k+1}$  is characterized by

$$\langle \underline{U}^{k+1}|_{\Gamma_d} - \underline{\psi}_d, \underline{V} \rangle_{\Gamma_d} + c \langle \underline{U}^{k+1} - \underline{U}^k, \underline{V} \rangle_{\Gamma} = 0, \quad \forall \underline{V} \in H(\Gamma). \quad (7)$$

### 3.2 Convergence of the sequence

**Lemma 1.** *The sequence  $\{\underline{U}^k\}_{k \geq 1}$  corresponding to the optimal elements retrieved verifies the following identity*

$$\|\underline{U}^{n+1} - \underline{\psi}_e\|_{\Gamma}^2 + \sum_{k=0}^n \|\underline{U}^{k+1} - \underline{U}^k\|_{\Gamma}^2 + \frac{2}{c} \sum_{k=0}^n \|\underline{U}^{k+1}|_{\Gamma_d} - \underline{\psi}_d\|_{\Gamma_d}^2 = \|\underline{U}^0 - \underline{\psi}_e\|_{\Gamma}^2, \quad \forall n \in \mathbb{N}^*, \quad (8)$$

where  $\underline{\psi}_e$  is the solution of the Cauchy problem given by Eqs. (1) and (2), and  $\underline{\psi}_d = \underline{\psi}_e|_{\Gamma_d}$ .

*Proof.* The following identity holds:

$$\begin{aligned} \|\underline{U}^{k+1} - \underline{\psi}_e\|_{\Gamma}^2 &= \langle (\underline{U}^{k+1} - \underline{U}^k) + (\underline{U}^k - \underline{\psi}_e), (\underline{U}^{k+1} - \underline{U}^k) + (\underline{U}^k - \underline{\psi}_e) \rangle_{\Gamma} \\ &= \|\underline{U}^{k+1} - \underline{U}^k\|_{\Gamma}^2 + \|\underline{U}^k - \underline{\psi}_e\|_{\Gamma}^2 + 2\langle \underline{U}^k - \underline{\psi}_e, \underline{U}^{k+1} - \underline{U}^k \rangle_{\Gamma} \\ &= \|\underline{U}^k - \underline{\psi}_e\|_{\Gamma}^2 - \|\underline{U}^{k+1} - \underline{U}^k\|_{\Gamma}^2 + 2\langle \underline{U}^{k+1} - \underline{\psi}_e, \underline{U}^{k+1} - \underline{U}^k \rangle_{\Gamma} \end{aligned} \quad (9)$$



Using the characterization (7) of  $\underline{U}^{k+1}$  with  $\underline{V} = \underline{U}^{k+1} - \underline{\psi}_e$  as a test function, one obtains

$$\langle \underline{U}^{k+1} - \underline{\psi}_e, \underline{U}^{k+1} - \underline{U}^k \rangle_\Gamma = -\frac{1}{c} \|\underline{U}^{k+1}|_{\Gamma_d} - \underline{\psi}_d\|_{\Gamma_d}^2. \quad (10)$$

Substituting relation (10) into (9) yields

$$\|\underline{U}^{k+1} - \underline{\psi}_e\|_\Gamma^2 + \|\underline{U}^{k+1} - \underline{U}^k\|_\Gamma^2 + \frac{2}{c} \|\underline{U}^{k+1}|_{\Gamma_d} - \underline{\psi}_d\|_{\Gamma_d}^2 = \|\underline{U}^k - \underline{\psi}_e\|_\Gamma^2.$$

Finally, by summing up the above relationship for  $k = \overline{0, n}$ , one obtains (8).  $\square$

**Theorem 1** (convergence of sequence  $\{\underline{U}^{k+1}\}_{k \geq 1}$ ). *Let  $\underline{\psi}_d$  be the compatible Cauchy data associated with the compatible pair  $\underline{\psi}_e = (u^e, \Phi^e) \in H(\Gamma)$ . Then, the sequence produced by the iterative scheme (6) converges strongly to  $\underline{\psi}_d$  on  $\Gamma_d$  and weakly to  $\underline{\psi}_e$  on  $\Gamma$ , respectively.*

*Proof.* (a) Strong convergence of sequence  $\{\underline{U}^k\}_{k \geq 1}$  to  $\underline{\psi}_d$  on  $\Gamma_d$ :

From (8) we derive that

$$\sum_{k=0}^n \|\underline{U}^{k+1} - \underline{\psi}_d\|_{\Gamma_d}^2 < \infty,$$

which immediately yields the strong convergence result

$$\lim_{k \rightarrow \infty} \|\underline{U}^{k+1} - \underline{\psi}_d\|_{\Gamma_d} = 0. \quad (11)$$

(b) Weak convergence of a subsequence of  $\{\underline{U}^k\}_{k \geq 1}$  to  $\underline{\psi}_e$  in  $H(\Gamma)$ :

From (8) we know that  $\{\underline{U}^k - \underline{\psi}_e\}_{k \geq 1}$  is a bounded sequence. The sequence  $\{\underline{U}^k\}_{k \geq 1}$  is therefore bounded in  $H(\Gamma)$ . Hence there exists a subsequence of  $\{\underline{U}^k\}_{k \geq 1}$ , denoted by  $\{\underline{U}^{m_k}\}_{k \geq 1}$ , which converges weakly in  $H(\Gamma)$ . Let  $\underline{U}$  be its limit. Our goal is to prove that  $\underline{U}|_{\Gamma_d} \equiv \underline{\psi}_d$ .

As a consequence of (11), the following relation holds

$$\lim_{k \rightarrow \infty} \|\underline{U}^{m_k}|_{\Gamma_d} - \underline{\psi}_d\|_{\Gamma_d} = 0$$

or, equivalently,

$$\lim_{k \rightarrow \infty} \underline{U}^{m_k}|_{\Gamma_d} = \underline{\psi}_d.$$

From the uniqueness of the limit on  $\Gamma_d$ , it follows that  $\underline{U}|_{\Gamma_d} = \underline{\psi}_d$ .

Next, from the uniqueness of the solution to the Cauchy problem associated with the Helmholtz equation [9], we obtain that  $\underline{U} \equiv \underline{\psi}_e$  on  $\Gamma$ .

(c) Weak convergence of sequence  $\{\underline{U}^k\}_{k \geq 1}$ :

By assuming the contrary, it follows that there exists  $\underline{V} \in H(\Gamma)$  and  $\epsilon > 0$  such that

$$\forall N \in \mathbb{N}, \exists n = n(N) > N \text{ such that } |\langle \underline{U}^n - \underline{\psi}_e, \underline{V} \rangle_{\Gamma}| \geq \epsilon.$$

This gives rise to a subsequence  $\{\underline{U}^{p_k}\}_{k \geq 1}$  such that

$$\forall p \in \mathbb{N}, |\langle \underline{U}^{p_k} - \underline{\psi}_e, \underline{V} \rangle_{\Gamma}| \geq \epsilon. \quad (12)$$

On the other hand,  $\{\underline{U}^{p_k}\}_{k \geq 1}$  is bounded in  $H(\Gamma)$  since  $\{\underline{U}^k\}_{k \geq 1}$  is bounded. It is thus possible to find out a subsequence of  $\{\underline{U}^{p_k}\}_{k \geq 1}$  which converges weakly on  $\Gamma$  and since  $\lim_{k \rightarrow \infty} \|\underline{U}^{p_k} - \underline{\psi}_d\|_{\Gamma_d} = 0$ , its limit is necessarily  $\underline{\psi}_e$ . This is in contradiction with relation (12) and hence it concludes the proof. □

### 3.3 Discrete formulation using the method of fundamental solutions (MFS)

Seeking the optimal element  $\underline{U}^{k+1}$  characterized by (7) requires to discretize the space  $H(\Omega)$  and herein this is accomplished by employing the method of fundamental solutions (MFS). The main idea of the MFS consists of approximating the solution in the domain  $\Omega$  and on its boundary  $\partial\Omega$  by a linear combination of fundamental solutions with respect to  $N$  source points  $\underline{y}^j \in \mathbb{R}^2 \setminus \overline{\Omega}$ ,  $j = \overline{1, N}$ , in the form

$$u(\underline{x}) \approx u^N(\underline{a}, \underline{Y}; \underline{x}) = \sum_{j=1}^N a_j \mathcal{F}(\underline{x}, \underline{y}^j), \quad \underline{x} \in \overline{\Omega}. \quad (13)$$

The fundamental solution  $\mathcal{F}$  of the Helmholtz equation (1) in the two-dimensional case is given by [38]:

$$\mathcal{F}(\underline{x}, \underline{y}) = \frac{i}{4} H_0^{(1)}(kr(\underline{x}, \underline{y})), \quad \underline{x} \in \overline{\Omega}, \quad \underline{y} \in \mathbb{R}^2 \setminus \overline{\Omega}. \quad (14)$$

Here  $i = \sqrt{-1}$ ,  $r(\underline{x}, \underline{y}) = \sqrt{(x_1 - y_1)^2 + (x_2 - y_2)^2}$  is the distance between the domain or boundary point  $\underline{x} = (x_1, x_2) \in \overline{\Omega}$  and the source point  $\underline{y} = (y_1, y_2) \in \mathbb{R}^2 \setminus \overline{\Omega}$ ,  $H_0^{(1)}$  is the Hankel function of the first kind of order zero,  $\underline{a} = (a_1, \dots, a_N)$  and  $\underline{Y}$  is the  $2N$ -vector containing the coordinates of the source points  $\underline{y}^j$ ,  $j = \overline{1, N}$ .

Then, the normal derivative on  $\Gamma$  can be approximated by

$$\Phi(\underline{x}) \approx \Phi^N(\underline{a}, \underline{Y}, \underline{n}; \underline{x}) = \sum_{j=1}^N a_j \mathcal{G}(\underline{x}, \underline{y}^j; \underline{n}), \quad \underline{x} \in \Gamma, \quad (15)$$

where  $\mathcal{G}(\underline{x}, \underline{y}^j; \underline{n}) = \nabla_{\underline{x}} \mathcal{F}(\underline{x}, \underline{y}) \cdot \underline{n}(\underline{x})$ , and in the case of the Helmholtz equation,  $\mathcal{G}$  is given by

$$\mathcal{G}(\underline{x}, \underline{y}; \underline{n}) = -\frac{((\underline{x} - \underline{y}) \underline{n}(\underline{x}))ki}{4r(\underline{x}, \underline{y})} H_1^{(1)}(kr(\underline{x}, \underline{y})), \quad \underline{x} \in \overline{\Omega}, \quad \underline{y} \in \mathbb{R}^2 \setminus \overline{\Omega}. \quad (16)$$

Here  $H_1^{(1)}$  is the Hankel function of the first kind of order one.

It should be noted that approximations (13) and (15) can also be written as

$$u(\underline{x}) \approx A(\underline{x})\underline{a}, \quad \underline{x} \in \overline{\Omega} \quad \text{and} \quad \Phi(\underline{x}) \approx B(\underline{x})\underline{a}, \quad \underline{x} \in \Gamma,$$

where  $A(\underline{x})$  and  $B(\underline{x})$  are matrices containing the fundamental solutions and their associated normal derivatives, respectively.

Further, according to the fading regularization algorithm described in Section 3.1, at each step  $k \geq 0$  of the minimization problem (6) or, equivalently, Eq. (7), one has to approximate both the known boundary data  $u^{(k)}|_{\Gamma_d}$  and  $\Phi^{(k)}|_{\Gamma_d}$  and the unknown boundary data  $u^{(k)}|_{\Gamma_u}$  and  $\Phi^{(k)}|_{\Gamma_u}$ , at the same time accounting for the given perturbed boundary conditions  $\tilde{u}^\varepsilon|_{\Gamma_d}$  and  $\tilde{\Phi}^\varepsilon|_{\Gamma_d}$ . To do this, we collocate the corresponding boundary conditions (2) at  $\{\underline{x}^{(m)}\}_{m=\overline{1, M_d}} \subset \Gamma_d$  and also express the MFS approximations (13) and (15) for the unknown solution and its normal derivative at  $\{\underline{x}^{(m)}\}_{m=\overline{M_d+1, M}} \subset \Gamma_u$ . Consequently, the iterative algorithm (6) is reduced to a sequence of linear minimization problems with respect to the corresponding unknown MFS constants  $\underline{a}$ , namely

$$\min_{\underline{a}} \mathcal{J}^{k+1}(\underline{a}) = \|S(\underline{x})\underline{a} - \tilde{U}^\varepsilon|_{\Gamma_d}\|_{\Gamma_d}^2 + c \|S(\underline{x})\underline{a} - S(\underline{x})\underline{a}^k\|_{\Gamma_u \cup \Gamma_d}^2, \quad (17)$$

where the matrix  $S$  is defined by  $S_{ij}(\underline{x}) = A_{ij}(\underline{x})$  and  $S_{(M+i)j}(\underline{x}) = B_{ij}(\underline{x})$  with  $i = \overline{1, M}$  and  $j = \overline{1, N}$ . Here  $\tilde{U}^\varepsilon|_{\Gamma_d} \in \mathbb{R}^{2M_d}$  contains the given perturbed boundary conditions  $\tilde{U}^\varepsilon|_{\Gamma_d} = (\tilde{u}^\varepsilon|_{\Gamma_d}, \tilde{\Phi}^\varepsilon|_{\Gamma_d})$ ,

whilst  $\underline{a}^k \in \mathbb{R}^N$  contains the MFS constants associated with the numerical solution of the discretised minimization problem (7) at the previous step  $k$ .

## 4 Numerical results and discussion

Herein we present the numerical results obtained using the fading regularization method and the MFS described in Sections 3.1 and 3.3, respectively. Various cases are considered for which an analytical solution  $u^{an}$  is known.

The following control quantities are used to estimate the accuracy of the proposed algorithm and the convergence of the iterative process:

- (i) the relaxation term in functional (6):

$$J_{\Gamma_d}(u^{k+1}, \Phi^{k+1}) = \|u^{k+1} - u^d\|_{\Gamma_d}^2 + \|\Phi^{k+1} - \Phi^d\|_{\Gamma_d}^2; \quad (18)$$

- (ii) the regularization term in functional (6):

$$J_{\Gamma}(u^{k+1}, \Phi^{k+1}) = c \|u^{k+1} - u^k\|_{\Gamma}^2 + c \|\Phi^{k+1} - \Phi^k\|_{\Gamma}^2; \quad (19)$$

- (iii) the value  $J(u^{k+1}, \Phi^{k+1}) = J_{\Gamma_d}(u^{k+1}, \Phi^{k+1}) + J_{\Gamma}(u^{k+1}, \Phi^{k+1})$  of functional (6) for the optimal element  $(u^{k+1}, \Phi^{k+1})$ ;

- (iv) the  $L^2$ -relative error in  $u$ :

$$u_{error} = \frac{\|u - u^{an}\|_{L^2(\Gamma)}}{\|u^{an}\|_{L^2(\Gamma)}}; \quad (20)$$

- (v) the  $L^2$ -relative error in  $\Phi$ :

$$\Phi_{error} = \frac{\|\Phi - \Phi^{an}\|_{L^2(\Gamma)}}{\|\Phi^{an}\|_{L^2(\Gamma)}}. \quad (21)$$

Three properties of the functional terms in the minimizing sequence can be easily established without the assumption that the data  $(u^d, \Phi^d)$  is compatible, namely

(a)  $J_{\Gamma_d}(u^{k+1}, \Phi^{k+1})$  is monotonically decreasing, i.e.

$$J_{\Gamma_d}(u^{k+1}, \Phi^{k+1}) \leq J_{\Gamma_d}(u^k, \Phi^k), \forall k \geq 0. \quad (22)$$

(b)  $J_{\Gamma}(u^{k+1}, \Phi^{k+1})$  is monotonically decreasing as soon as  $c > 0$ , i.e.

$$J_{\Gamma}(u^{k+1}, \Phi^{k+1}) \leq J_{\Gamma}(u^k, \Phi^k), \forall k \geq 0. \quad (23)$$

(c) The sequence defined by the values of the functional  $J$  for each optimal element  $(u^{k+1}, \Phi^{k+1})$  is also monotonically decreasing as soon as  $c > 0$ , i.e.

$$J(u^{k+1}, \Phi^{k+1}) \leq J(u^k, \Phi^k), \forall k \geq 0. \quad (24)$$

In all examples considered herein, we have taken  $M_d$  and  $M_u$  uniformly distributed collocation points on  $\Gamma_d$  and  $\Gamma_u$ , respectively, as well as  $N$  uniformly distributed sources. It should be mentioned that the sources are preassigned and kept fixed throughout the solution process on a pseudo-boundary  $\tilde{\Gamma}$  of a similar shape to that of  $\Gamma$  such that  $\text{dist}(\tilde{\Gamma}, \Gamma)$  is a fixed constant (i.e. the so-called static MFS approach has been employed) [43].

#### 4.1 Example 1

We consider the following analytical solution:

$$u^{an}(\underline{x}) = \cos\left(\frac{1}{2}x_1 + \frac{\sqrt{3}}{2}x_2\right), \quad \underline{x} = (x_1, x_2) \in \Omega, \quad (25)$$

in the unit disk  $\Omega = \{\underline{x} = (x_1, x_2) | x_1^2 + x_2^2 < 1\}$ , where  $k^2 = 1$ . Here  $\Gamma_d = \{\underline{x} \in \Gamma | 0 \leq \theta(\underline{x}) \leq \pi\}$  and  $\Gamma_u = \{\underline{x} \in \Gamma | \pi \leq \theta(\underline{x}) \leq 2\pi\}$ , where  $\theta(\underline{x})$  is the angular polar coordinate of  $\underline{x}$ .

The corresponding MFS parameters have been set as:

$N = 10$  on  $\tilde{\Gamma} = \{\underline{x} = (x_1, x_2) \in \mathbb{R}^2 | x_1^2 + x_2^2 = d^2\}$  and  $d = 10$ , whilst  $M_d = M_u = 150$ . Note that  $\text{meas}(\Gamma_d) = \text{meas}(\Gamma_u) = \frac{1}{2}\text{meas}(\Gamma)$ .

#### 4.1.1 Stopping criterion

For both exact and noisy Cauchy data, a stopping criterion is needed to stop the iterative process before the iteration number at which the contribution of noise in the data to the numerical solution becomes significant and hence the latter becomes oscillatory/unstable. In the present case, the data on  $\Gamma_d$  are generated from the analytical solution  $u^{an}$  (25) and its associated normal derivative  $\Phi^{an}$  and are not blurred.

Figure 2 represents the evolution of the control quantities  $J(u^{k+1}, \Phi^{k+1})$ ,  $J_{\Gamma_d}(u^{k+1}, \Phi^{k+1})$  and  $J_{\Gamma}(u^{k+1}, \Phi^{k+1})$  versus the number of iterations  $k$  for  $c = 1.10^{-2}$ . We note that from the 86<sup>th</sup> iteration the quantities  $J(u^{k+1}, \Phi^{k+1})$  and  $J_{\Gamma_d}(u^{k+1}, \Phi^{k+1})$ , as well as the errors  $u_{error}$  and  $\Phi_{error}$  remain constant. We also observe that the method converges.

The iteration at which the iterative process is stopped, is determined by using the quantity  $J_{\Gamma}(u^{k+1}, \Phi^{k+1})$ , where  $(u^{k+1}, \Phi^{k+1})$  is the optimal element obtained at the  $(k+1)^{th}$  step. As expected, the control quantity  $J_{\Gamma}$  decreases for  $k < 86$  and then becomes constant with only a few oscillations caused by numerical approximations for  $k > 86$ . We search for the step  $k_{opt}$  where the regularization term  $J_{\Gamma}$  increases, i.e  $J_{\Gamma}(u^{k+1}, \Phi^{k+1}) > J_{\Gamma}(u^k, \Phi^k)$ , and hence the iterative process is stopped at  $k_{opt} = 86$ . This stopping criterion is blind because, when calculating the quantity  $J_{\Gamma}$ , we do not need to know the analytical solution. Indeed, one only needs to know two successive optimal elements.

We observe that oscillations occur in the term  $J_{\Gamma}$  because of numerical approximations, however this term becomes negligible compared to  $J_{\Gamma_d}$  and tends to zero. This proves that the algorithm converges indeed. The residual error  $J_{\Gamma_d}$  (relaxation term) and the term  $J$  decrease during the iterative process. After convergence is achieved, the relaxation term  $J_{\Gamma_d}$  remains constant and this corresponds to the numerical approximation error.

It can also be observed that, as expected, the errors in the numerical normal derivative ( $\Phi_{error}$ ), obtained using the iterative method, are larger than those corresponding to the reconstructed solution ( $u_{error}$ ).

#### 4.1.2 Influence of parameter $c$

It is necessary to investigate the influence of parameter  $c$ , which defines the relative weight of the regularization term  $J_\Gamma$  compared to the relaxation term  $J_{\Gamma_d}$ , on the accuracy of the numerical solution and the number of iterations performed. Figures 3(a) and (b) show the reconstructions of the solution and its normal derivative on  $\Gamma$ , for various values of  $c$ , respectively.

It can be seen from Table 1, that the choice of parameter  $c$  affects the number of iterations  $k$  required to obtain convergence. Table 1 lists the results, obtained for a large range of regularization parameter  $c$ , by specifying the number of iterations necessary to achieve convergence and the errors  $u_{error}$  and  $\Phi_{error}$ . We also mention that all numerical computations have been performed on a machine with a 2.90GHz Intel® Core™ i7-4910MQ. The errors in  $u$  and  $\Phi$  are identical for each value of parameter  $c$  listed in Table 1 and this confirms that the algorithm converges to the same solution, regardless the value of  $c$ .

Figure 4 shows the evolution of the control quantities introduced in Eqs. (18) and (19) versus  $\frac{k}{c}$  for three values of  $c$ . We notice that, for each  $c$ , the relaxation term in functional (18) remains constant as the number of iterations required to achieve convergence is reached. Furthermore,  $J_{\Gamma_d}$  has almost the same value in this case, see Figure 4(a).

Analogous and for comparison purposes, Figure 5 shows the evolution of the terms introduced by Eqs. (20) and (21), as functions of  $\frac{k}{c}$  for various values of  $c$ . Each quantity tends to the same value, see Figures 5(a) and (b), and the errors in  $u$  and  $\Phi$  are quite identical for each value of  $c$ .

#### 4.1.3 Reconstruction with noisy data $\underline{\psi}_d$

Next, we investigate how the reconstructions are influenced by noisy data. We assume that the given exact boundary data  $\tilde{u}|_{\Gamma_d} = u^{an}|_{\Gamma_d}$  and  $\tilde{\Phi}|_{\Gamma_d} = \Phi^{an}|_{\Gamma_d}$  have been perturbed as

$$\begin{aligned}\tilde{u}^\varepsilon(\underline{x}) &= u^{an}(\underline{x}) + \delta u^{an}(\underline{x}) \cdot \rho, \quad \underline{x} \in \Gamma_d, \\ \tilde{\Phi}^\varepsilon(\underline{x}) &= \Phi^{an}(\underline{x}) + \delta \Phi^{an}(\underline{x}) \cdot \rho, \quad \underline{x} \in \Gamma_d,\end{aligned}\tag{26}$$

where  $\delta$  is the level of percentage noise added to  $\tilde{u}|_{\Gamma_d} = u^{an}|_{\Gamma_d}$  and  $\tilde{\Phi}|_{\Gamma_d} = \Phi^{an}|_{\Gamma_d}$ , respectively, and  $\rho$  is a pseudo-random number drawn from the standard uniform distribution in  $[-1, 1]$ .

The reconstructions of  $u$  and  $\Phi$  on  $\Gamma$ , obtained with the noise level of 1%, 3%, 5% and 10%, are represented in Figures 6(a) and (b), respectively. It can be seen from these figures that the reconstructions are very accurate.

Table 2 tabulates the results obtained for various levels of noise and various values of  $c$ , by specifying the number of iterations necessary to achieve convergence and the errors  $u_{error}$  and  $\Phi_{error}$ . For each noise level, the errors in  $u$  and  $\Phi$  do not depend on the values of parameter  $c$ . This shows that even for noisy data, the numerical reconstructions are also independent of  $c$  and, therefore, the combined fading regularization method-MFS algorithm is, at the same time, robust.

Figure 7 represents the evolution of the control errors  $J_{\Gamma_d}(u^{k+1}, \Phi^{k+1})$ ,  $J_{\Gamma}(u^{k+1}, \Phi^{k+1})$  and the errors  $u_{error}$  and  $\Phi_{error}$  versus  $\frac{k}{c}$ , for various values of  $c$  and  $\delta = 10\%$ . We note that, for each  $c$ , the regularization term  $J_{\Gamma}$  is monotonically decreasing and the relaxation term  $J_{\Gamma_d}$  remains constant as the number of iterations required to achieve convergence is reached. We observe that the minima reached are the same for different values of parameter  $c$  (Figures 7(c) and (d)) and as  $c$  increases, the number of iterations  $k$ , given by the stopping criterion, becomes more important. This shows that the solution is independent of the parameter  $c$ , which is just a convergence accelerator.

The stopping criterion, defined in Section 4.1.1, is still valid since it leads us to choosing a stable solution, but it does not allow us to achieve the optimal one. The regularization term  $J_{\Gamma}$  is negligible and hence the residual term  $J$  is equal to the relaxation term  $J_{\Gamma_d}$ . The latter term corresponds to the distance on  $\Gamma_d$  between the deblurred reconstruction and the noisy data and therefore, gives us information on the level of noise in the data.

Figures 8(a) and (b) show the reconstructions, on  $\Gamma_d$ , of the solution  $u$  and its normal derivative  $\Phi$ , respectively, obtained with  $c = 1.10^{-1}$  and 10% noise in  $\tilde{u}^{\varepsilon}$  and  $\tilde{\Phi}^{\varepsilon}$ . The reconstructions obtained for both  $u|_{\Gamma_u}$  and  $\Phi|_{\Gamma_u}$  can be seen to be very accurate. Functional (6) is composed of two terms with different roles. As in most inverse iterative methods, there is a regularization term which tends



to zero as iterations increase. However, in the present method, there is also a relaxation term that allows for the data blurred by noise to be taken into account. Therefore, we seek a solution which is close to the data, but not a solution that exactly fits the data. The algorithm then recomputes, at each step, a solution on the whole boundary. It can be noticed that these reconstructions correspond to the analytical solutions  $u^{an}$  and  $\Phi^{an}$  and that the noise level in the data has been filtered out by the present algorithm.

#### 4.1.4 Influence of the number of sources

Herein we investigate the influence of the number of sources,  $N$ , on the numerical reconstructions of  $u|_{\Gamma_u}$  and  $\Phi|_{\Gamma_u}$ .

Figures 9(a) and (b) show the reconstructions, on  $\Gamma$ , of the solution  $u$  and its normal derivative  $\Phi$ , respectively, obtained with the stopping criterion introduced in Section 4.1.1,  $M_d = M_u = 150$ ,  $d = 10$ ,  $\delta = 3\%$ ,  $c = 1.10^{-1}$  and  $N \in \{5, 10, 20, 40\}$ . It can be observed that the number of sources  $N$  affects these reconstructions. Better convergence is achieved by the MFS discretisation when using  $N = 10$  source points, see also Table 3.

#### 4.1.5 Influence of the distance from the sources to the boundary of the solution domain

Next, we discuss the sensitivity of the numerical results obtained with respect to the distance from the sources to the boundary of the domain.

Figures 10(a) and (b) show the reconstruction, on  $\Gamma$ , of the solution  $u$  and its normal derivative  $\Phi$ , respectively, obtained when applying the fading regularization-MFS algorithm, the stopping criterion introduced in Section 4.1.1,  $N = 10$ ,  $M_d = M_u = 150$ ,  $\delta = 3\%$ ,  $c = 1.10^{-1}$  and various values of  $d$ . It can be observed from these figures that the numerical solution and the corresponding normal derivative are not affected by the position of the sources, as they are far enough from the boundary of the domain (i.e. for  $d \geq 5$ ). For  $d < 5$  the reconstructions are less accurate, however still good, see also Table 4.

Table 4 displays the results obtained for various values of  $d$  by specifying the number of iterations

necessary to achieve convergence and the errors  $u_{error}$  and  $\Phi_{error}$ . We notice that the position of source points affects the results if  $1.5 \leq d < 5$ . When  $d \geq 5$ , the errors in  $u$  and  $\Phi$  are quite identical, whilst for sufficiently large values of  $d$  ( $d \geq 40$ ), these errors become almost constant.

## 4.2 Example 2

A similar study is further performed for the Cauchy problem associated with the Helmholtz equation in the unit square. We consider the following analytical solution in  $\Omega = (0, 1)^2$  with  $k^2 = 4$ :

$$u^{an}(\underline{x}) = \cos(x_1 + \sqrt{3}x_2), \quad \underline{x} = (x_1, x_2) \in \Omega. \quad (27)$$

Here  $\Gamma_d = \{\underline{x} \in \Gamma | 0 \leq x_1 \leq 1, x_2 = 0\} \cup \{\underline{x} \in \Gamma | x_1 = 1, 0 \leq x_2 \leq 1\}$  and  $\Gamma_u = \{\underline{x} \in \Gamma | 0 \leq x_1 \leq 1, x_2 = 1\} \cup \{\underline{x} \in \Gamma | x_1 = 0, 0 \leq x_2 \leq 1\}$ .

According to the notations used in Section 3.3, the corresponding MFS parameters have been set as  $N = 10$  on  $\tilde{\Gamma} = \{\underline{x} = (x_1, x_2) \in \mathbb{R}^2 \mid x_1^2 + x_2^2 = d^2\}$  and  $d = 10$ , whilst  $M_d = M_u = 100$ . Note that  $\text{meas}(\Gamma_d) = \text{meas}(\Gamma_u) = \frac{1}{2}\text{meas}(\Gamma)$ .

Figures 12(a) and (b) show the analytical solution and the numerical reconstruction for  $u$  and the normal derivatives  $\Phi$ , respectively, for  $\delta \in \{1\%, 3\%, 5\%, 10\%\}$  and  $c = 1$ . It can be remarked from these figures the accuracy of the reconstructions on  $\Gamma_u$  and the capability of the fading regularization-MFS algorithm to deblur the noisy data on  $\Gamma_d$ . We also notice the accurate reconstructions (see also Table 5) when the boundary  $\Gamma_u$  is piecewise smooth (i.e. it has corners). The numerical results presented in Figures 12(a) and (b) correspond to  $c = 1$ , but one can take a lower value for the regularization parameter to speed up the convergence.

Next, we investigate the influence of the number of sources on the numerical reconstruction of the boundary data. Figure 13 shows the reconstructions of the solution and its normal derivative on  $\Gamma$ , obtained for  $N \in \{4, 6, 10, 50\}$ . We can observe that these reconstructions are very bad approximations for their corresponding analytical values for  $N = 4$  (too low number of sources) and  $N = 50$  (too large number of sources). We point out that  $\Phi_{error}$  is larger than  $u_{error}$  and this is due to the dramatic

change in the outward unit normal near the corners of the solution domain.

### 4.3 Example 3

As a final example, we consider the annular domain  $\Omega = \{\underline{x} \in \mathbb{R}^2 \mid R_{int} < \|\underline{x}\| < R_{out}\}$ , where  $R_{int} = 1.0$  and  $R_{out} = 2.0$ , which is bounded by the inner  $\Gamma_u = \{\underline{x} \in \mathbb{R}^2 \mid \|\underline{x}\| = R_{int}\}$  and the outer boundaries  $\Gamma_d = \{\underline{x} \in \mathbb{R}^2 \mid \|\underline{x}\| = R_{out}\}$ , respectively, and the following analytical solution:

$$u^{an}(\underline{x}) = \frac{i}{4} H_0^{(1)}(kr(\underline{x}, \underline{z})), \quad \underline{x} \in \overline{\Omega}, \quad \underline{z} \in \mathbb{R}^2 \setminus \overline{\Omega}. \quad (28)$$

Here  $k = 2$ ,  $r(\underline{x}, \underline{z}) = \sqrt{(x_1 - z_1)^2 + (x_2 - z_2)^2}$  represents the distance between the domain or boundary point  $\underline{x} = (x_1, x_2)$  and the singularity position  $\underline{z} = (z_1, z_2)$  with  $z_1 = 0.02$  and  $z_2 = -0.80$ , and  $H_0^{(1)}$  is the Hankel function of the first kind of order zero. The singularity position  $\underline{z}$  is chosen so that it is close enough to the boundary  $\Gamma_u$  in order to feel its influence.

The corresponding MFS parameters have been set as  $N = N_{out} + N_{int}$ ,  $N_{out} = 10$  on  $\tilde{\Gamma}_{out} = \{\underline{x} = (x_1, x_2) \in \mathbb{R}^2 \mid x_1^2 + x_2^2 = d_1^2\}$ ,  $d_1 = 5$ ,  $N_{int} = 30$  on  $\tilde{\Gamma}_{int} = \{\underline{x} = (x_1, x_2) \in \mathbb{R}^2 \mid x_1^2 + x_2^2 = d_2^2\}$  and  $d_2 = 0.5$ , whilst  $M_d = M_u = 150$  on both  $\Gamma_d$  and  $\Gamma_u$ .

The reconstructions of  $u$  and  $\Phi$  on  $\Gamma_u$  obtained with various noise levels, are represented in the Figures 15(a) and (b), respectively. It can be seen from these figures that these reconstructions are accurate despite the singular solution.

Figures 16(a) and (b) present the exact and numerical values for  $u|_{\Gamma_d}$  and  $\Phi|_{\Gamma_d}$ , respectively, obtained using  $\delta = 10\%$ , and it can be easily noticed the stability of the proposed algorithm in the case of Example 3.

## 5 Conclusion

In this paper, we have studied the numerical reconstruction of the missing solution and associated normal derivative on an inaccessible part of the boundary for the two-dimensional Helmholtz equation, from overprescribed noisy data taken on the remaining accessible boundary part. Three examples were

considered and thoroughly investigated by combining the fading regularization method presented in Section 3.1 with the MFS described in Section 3.3. The iterative procedure was stopped according to the stopping criterion introduced in Section 4.1.1. Numerical simulations have highlighted the efficiency, accuracy, convergence, stability and robustness of the algorithm to noisy data, as well as its ability to deblur noisy data.

For all situations analysed, it was observed that the errors in the numerical normal derivatives, obtained using the fading regularization-MFS algorithm, were higher than those corresponding to the reconstructed solutions. In addition to computing the solution on the underspecified boundary, the algorithm was also used to recompute the given noisy data, in the sense that the latter was denoised. For all examples considered, i.e. simply and doubly connected domains with (piecewise) smooth boundaries, as well as solutions with singularities, accurate reconstructions of the solution and its normal derivative have been retrieved. The solution was shown to be independent of the regularization parameter  $c$ , however the quality of the reconstructions was influenced by the choice of the number of sources and their position.

Future extension of the fading regularization-MFS algorithm is currently under investigation and refers to inverse boundary value problems associated with the two-dimensional Helmholtz equation for the detection of acoustic sources.

## Acknowledgements

L. Caillé, F. Delvare and L. Marin would like to acknowledge the financial support received from L.E.A.–Math Mode. The financial support received by L. Caillé from Région Normandie is also gratefully acknowledged.

## References

- [1] D.E. Beskos. Boundary element methods in dynamic analysis. *Applied Mechanics Reviews*, 40:1, 1987.
- [2] J.T. Chen and F.C. Wong. Dual formulation of multiple reciprocity method for the acoustic mode of a cavity with a thin partition. *Journal of Sound and Vibration*, 217(1):75–95, 1998.
- [3] I. Harari, P.E. Barbone, M. Slavutin, and R. Shalom. Boundary infinite elements for the Helmholtz equation in exterior domains. *International Journal for Numerical Methods in Engineering*, 41(6):1105–1131, 1998.
- [4] W.S. Hall and X.Q. Mao. A boundary element investigation of irregular frequencies in electromagnetic scattering. *Engineering Analysis with Boundary Elements*, 16(3):245–252, 1995.
- [5] J.P. Agnantiaris, D. Polyzos, and D.E. Beskos. Three-dimensional structural vibration analysis by the dual reciprocity BEM. *Computational Mechanics*, 21(4-5):372–381, 1998.
- [6] Y. Niwa, S. Kobayashi, and M. Kitahara. Determination of eigenvalue by boundary element method. *Development in Boundary Element Methods*, 1982.
- [7] A.J. Nowak and C.A. Brebbia. Solving Helmholtz equation by boundary elements using multiple reciprocity method. In *Computer Experiment in Fluid Flow*, pages 265–270. 1989.
- [8] J. Hadamard. *Lectures on Cauchy Problem in Linear Partial Differential Equations*. Oxford University Press, 1923.
- [9] A. Kirsch and F. Hettlich. *The Mathematical Theory of Time-Harmonic Maxwell's Equations*. Applied Mathematical Sciences, 2015.
- [10] M.R. Bai. Application of BEM-based acoustic holography to radiation analysis of sound sources with arbitrarily shaped geometries. *The Journal of the Acoustical Society of America*, 92(1):533–549, 1992.

- [11] B.-K. Kim and J.-G. Ih. On the reconstruction of the vibro-acoustic field over the surface enclosing an interior space using the Boundary Element Method. *The Journal of the Acoustical Society of America*, 100(5):3003–3016, 1996.
- [12] Z. Wang and S.F. Wu. Helmholtz equation–least-squares method for reconstructing the acoustic pressure field. *The Journal of the Acoustical Society of America*, 102(4):2020–2032, 1997.
- [13] S.R. Wu and J. Yu. Application of BEM-based acoustic holography to radiation analysis of sound sources with arbitrarily shaped geometries. *The Journal of the Acoustical Society of America*, 104(4):2054–60, 1998.
- [14] T. DeLillo, V. Isakov, N. Valdivia, and L. Wang. The detection of the source of acoustical noise in two dimensions. *SIAM Journal on Applied Mathematics*, 61(6):2104–2121, 2001.
- [15] L. Marin, L. Elliott, P.J. Heggs, D.B. Ingham, D. Lesnic, and X. Wen. An alternating iterative algorithm for the Cauchy problem associated to the Helmholtz equation. *Computer Methods in Applied Mechanics and Engineering*, 192(5):709–722, 2003.
- [16] L. Marin, L. Elliott, P.J. Heggs, D.B. Ingham, D. Lesnic, and X. Wen. Conjugate gradient-boundary element solution to the Cauchy problem for Helmholtz-type equations. *Computational Mechanics*, 31(3-4):367–377, 2003.
- [17] L. Marin, L. Elliott, P.J. Heggs, D.B. Ingham, D. Lesnic, and X. Wen. BEM solution for the Cauchy problem associated with Helmholtz-type equations by the Landweber method. *Engineering Analysis with Boundary Elements*, 28(9):1025–1034, 2004.
- [18] L. Marin. Boundary element-minimal error method for the Cauchy problem associated with Helmholtz-type equations. *Computational Mechanics*, 44(2):205–219, 2009.
- [19] L. Marin and D. Lesnic. The method of fundamental solutions for the Cauchy problem associated with two-dimensional Helmholtz-type equations. *Computers & Structures*, 83(4):267–278, 2005.

- [20] L. Marin. A meshless method for the numerical solution of the Cauchy problem associated with three-dimensional Helmholtz-type equations. *Applied Mathematics and Computation*, 165(2):355–374, 2005.
- [21] B. Jin and L. Marin. The plane wave method for inverse problems associated with Helmholtz-type equations. *Engineering Analysis with Boundary Elements*, 32(3):223–240, 2008.
- [22] L. Marin, L. Elliot, P.J. Heggs, D.B Ingham, D. Lesnic, and X. Wen. Dual reciprocity boundary element method solution of the Cauchy problem for Helmholtz-type equations with variable coefficients. *Journal of Sound and Vibration*, 297(1–2):89–105, 2006.
- [23] H.H. Qin, T. Wei, and R. Shi. Modified Tikhonov regularization method for the Cauchy problem of the Helmholtz equation. *Journal of Computational and Applied Mathematics*, 224:39–53, 2009.
- [24] H.H. Qin and T. Wei. Two regularization methods for the Cauchy problems of the Helmholtz equation. *Applied Mathematical Modelling*, 34:947–967, 2010.
- [25] S.I. Kabanikhin, Y.S. Gasimov, D.B. Nurseitsov, M.A. Shishlenin, B.B. Sholpanbaev, and S. Kasenov. Regularization of the continuation problem for elliptic equations. *Inverse and Ill-Posed Problems*, 21:871–884, 2013.
- [26] F. Berntsson, V.A. Kozlov, B. Mpinganzima, and O. Turesson. An alternating iterative procedure for the Cauchy problem for the Helmholtz equation. *Inverse Problems in Science and Engineering*, 22:45–62, 2014.
- [27] F. Berntsson, V.A. Kozlov, B. Mpinganzima, and O. Turesson. An accelerating alternating iterative procedure for the Cauchy problem for the Helmholtz equation. *Computers & Mathematics with Applications*, 68(1):44–60, 2014.
- [28] A. Cimetière, F. Delvare, M. Jaoua, and F. Pons. Solution of the Cauchy problem using iterated Tikhonov regularization. *Inverse Problems*, 17(3):553, 2001.

- [29] A. Cimetière, F. Delvare, and F. Pons. Une méthode inverse à régularisation évanescence [An inverse method with vanishing regularization]. *Comptes Rendus de l'Académie des Sciences-Series IIB-Mechanics*, 328(9):639–644, 2000.
- [30] F. Delvare, A. Cimetière, and F. Pons. An iterative boundary element method for Cauchy inverse problems. *Computational Mechanics*, 28(3-4):291–302, 2002.
- [31] A. Cimetière, F. Delvare, M. Jaoua, and F. Pons. An inversion method for harmonic functions reconstruction. *International Journal of Thermal Sciences*, 41(6):509–516, 2002.
- [32] F. Delvare and J.-L. Hanus. Complétion de données par méthode inverse en élasticité linéaire [Data completion using an inverse method in linear elasticity]. In *7ème Colloque National en Calcul de Structures*. Giens, France, mai 2005.
- [33] F. Delvare, A. Cimetière, J.-L. Hanus, and P. Bailly. An iterative method for the Cauchy problem in linear elasticity with fading regularization effect. *Computer Methods in Applied Mechanics and Engineering*, 199(49):3336–3344, 2010.
- [34] B. Durand, F. Delvare, and P. Bailly. Numerical solution of Cauchy problems in linear elasticity in axisymmetric situations. *International Journal of Solids and Structures*, 48(21):3041–3053, 2011.
- [35] L. Marin, F. Delvare, and A. Cimetière. Fading regularization MFS algorithm for inverse boundary value problems in two-dimensional linear elasticity. *International Journal of Solids and Structures*, 78–79:9–20, 2016.
- [36] V.D. Kupradze and M.A. Aleksidze. The method of functional equations for the approximate solution of certain boundary value problems. *USSR Computational Mathematics and Mathematical Physics*, 4(4):82–126, 1964.
- [37] R. Mathon and R.L. Johnston. The approximate solution of elliptic boundary-value problems by fundamental solutions. *SIAM Journal on Numerical Analysis*, 14(4):638–650, 1977.



- [38] G. Fairweather and A. Karageorghis. The method of fundamental solutions for elliptic boundary value problems. *Advances in Computational Mathematics*, 9(1-2):69–95, 1998.
- [39] M.A. Goldberg and C.S. Chen. The method of fundamental solutions for potential, Helmholtz and diffusion problems. In *Boundary Integral Methods-Numerical and Mathematical Aspects*, pages 103–176. 1999.
- [40] A. Karageorghis, D. Lesnic, and L. Marin. A survey of applications of the MFS to inverse problems. *Inverse Problems in Science and Engineering*, 19(3):309–336, 2011.
- [41] Q.G. Liu and B. Šarler. Non-singular method of fundamental solutions for anisotropic elasticity. *Engineering Analysis with Boundary Elements*, 45:68–78, 2014.
- [42] G. Chen and J. Zhou. *Boundary Element Methods*. Academic Press, 1992.
- [43] P. Gorzelańczyk and J.A. Kołodziej. Some remarks concerning the shape of the source contour with application of the method of fundamental solutions to elastic torsion of prismatic rods. *Engineering Analysis with Boundary Elements*, 32(1):64–75, 2008.

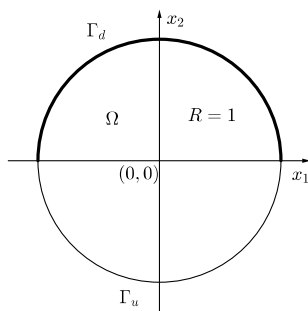


Figure 1: Schematic diagram of Example 1.

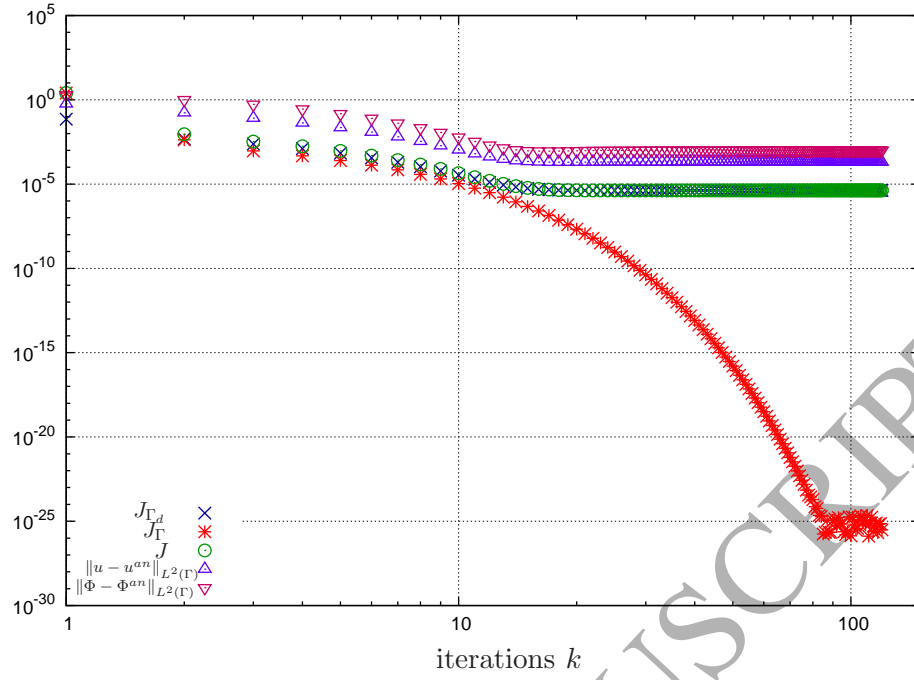


Figure 2: Evolution of the control terms with respect to the number of iterations,  $k$ , for  $c = 1.10^{-2}$ .

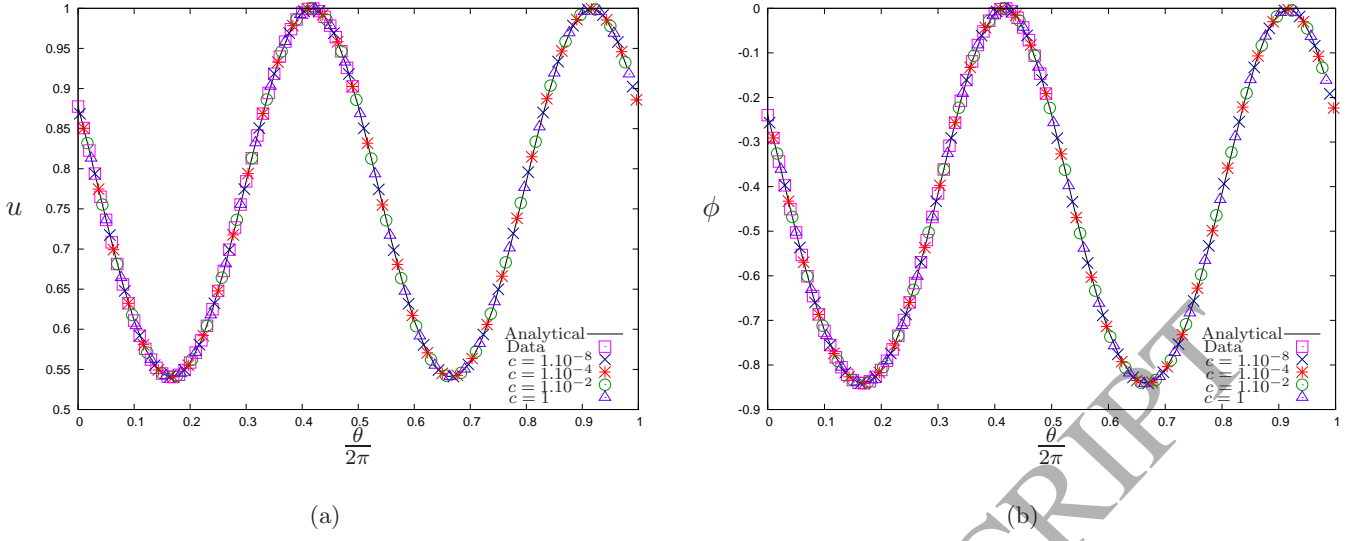
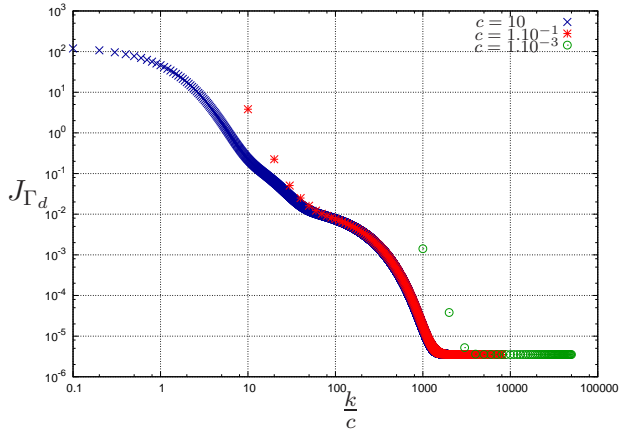
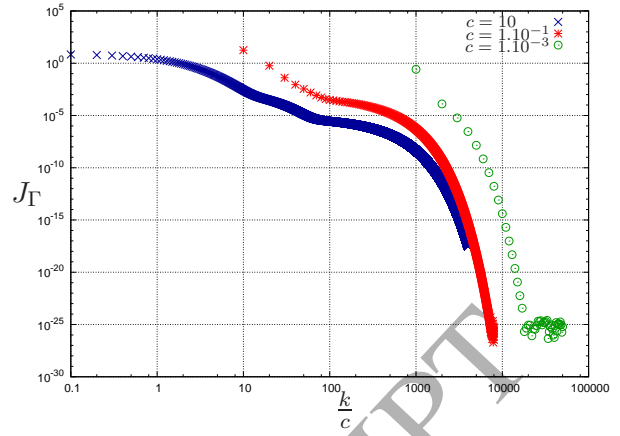


Figure 3: (a) The analytical,  $u^{an}$ , and the numerical solutions,  $u$ , and (b) the analytical,  $\phi^{an}$ , and the numerical normal derivatives,  $\phi$ , retrieved on the boundary  $\Gamma$ , for various values of  $c$ .



(a)



(b)

Figure 4: Evolution of the norms (a)  $J_{\Gamma_d} = \|u - u_d\|_{\Gamma_d}^2 + \|\Phi - \Phi_d\|_{\Gamma_d}^2$ , and (b)  $J_{\Gamma} = c\|u - u^{(k-1)}\|_{\Gamma}^2 + c\|\Phi - \Phi^{(k-1)}\|_{\Gamma}^2$ , as functions of  $\frac{k}{c}$ , for various values of  $c$ .

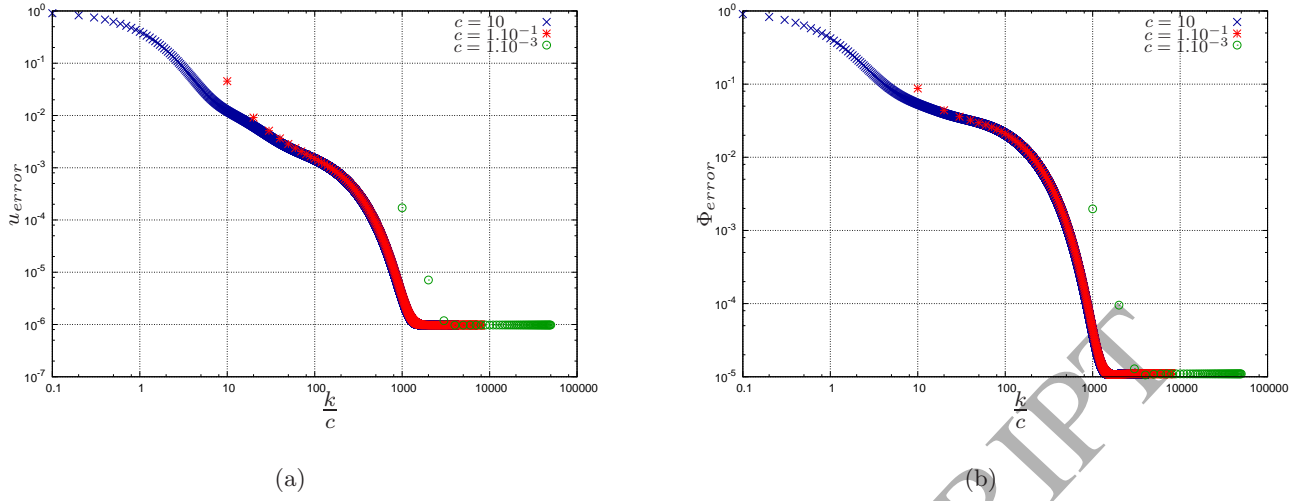


Figure 5: Evolution of the errors (a)  $u_{error}$ , and (b)  $\Phi_{error}$ , as functions of  $\frac{k}{c}$ , for various values of  $c$ .

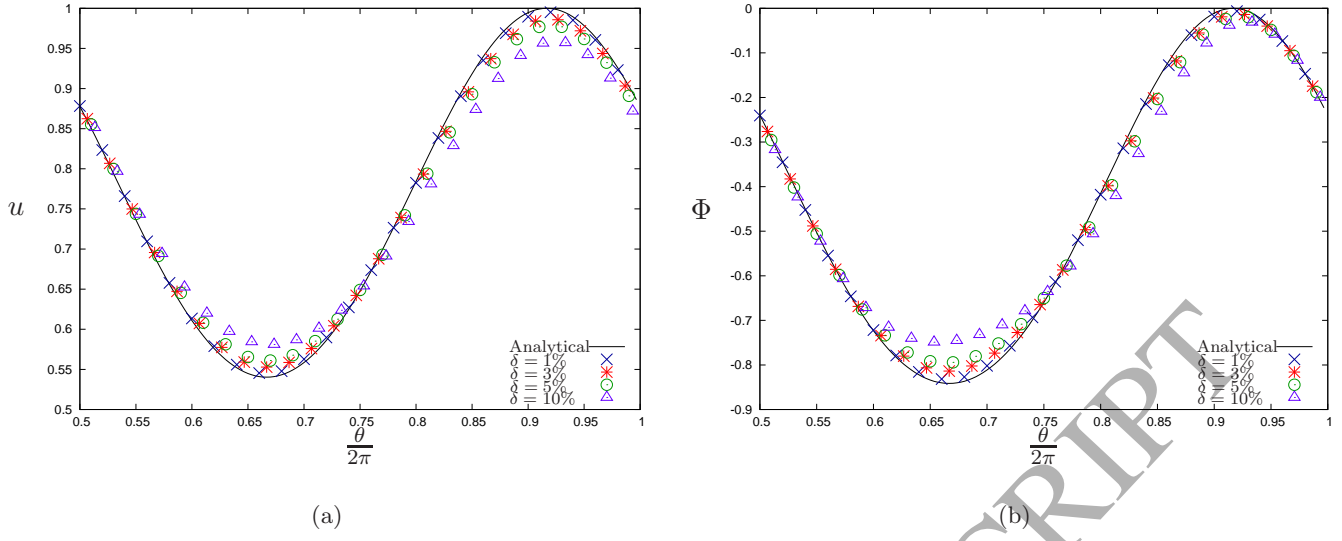


Figure 6: Reconstructions of (a) the solution  $u$ , and (b) its normal derivative  $\Phi$  on  $\Gamma$ , for various levels of noise and  $c = 1.10^{-1}$ .

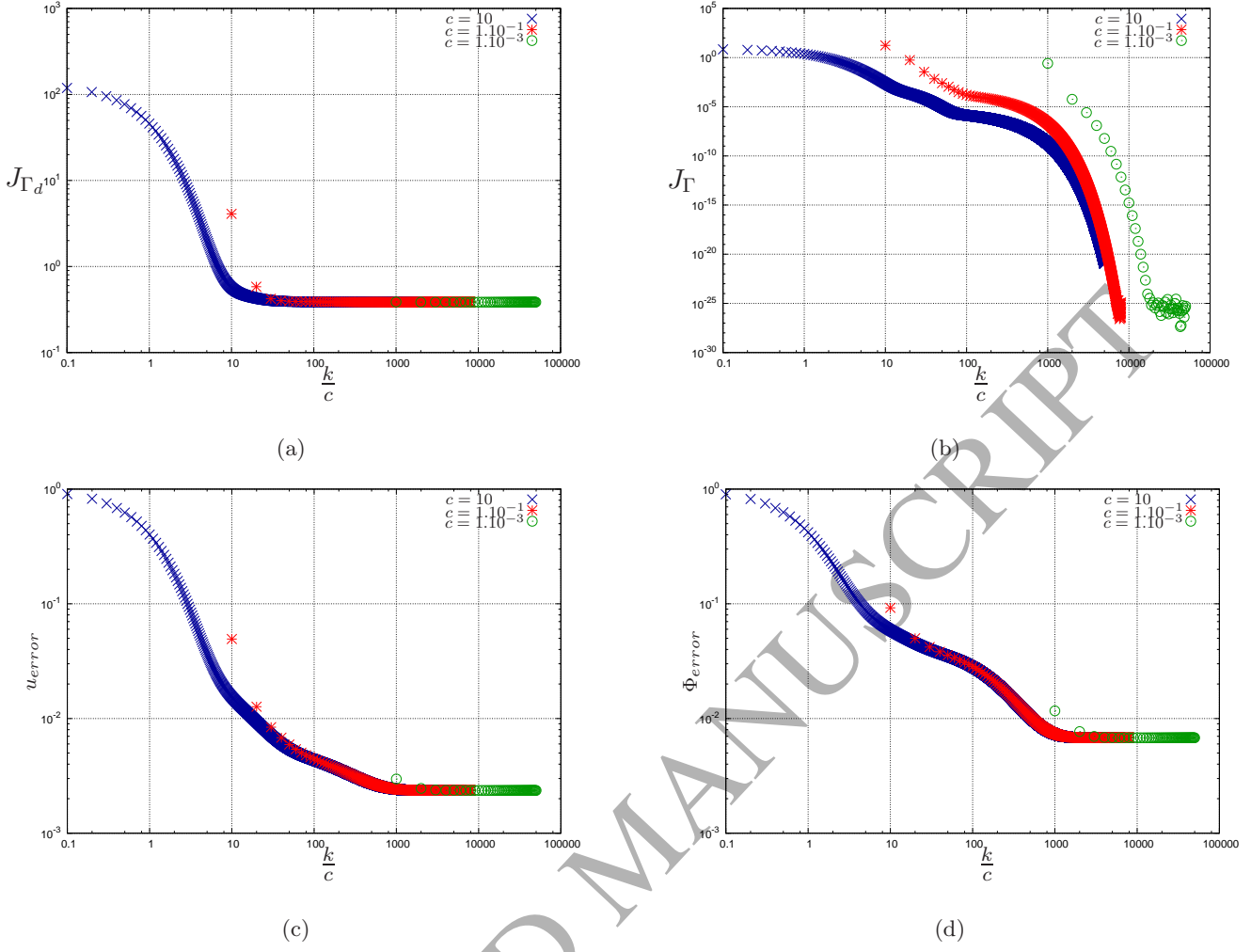


Figure 7: Evolution of the norms (a)  $J_{\Gamma_d} = \|u - u_d\|_{\Gamma_d}^2 + \|\Phi - \Phi_d\|_{\Gamma_d}^2$ , and (b)  $J_{\Gamma} = c\|u - u^{(k-1)}\|_{\Gamma}^2 + c\|\Phi - \Phi^{(k-1)}\|_{\Gamma}^2$ , and the errors (c)  $u_{error}$  and (d)  $\Phi_{error}$ , as functions of  $k/c$ , for various values of  $c$  and  $\delta = 10\%$ .



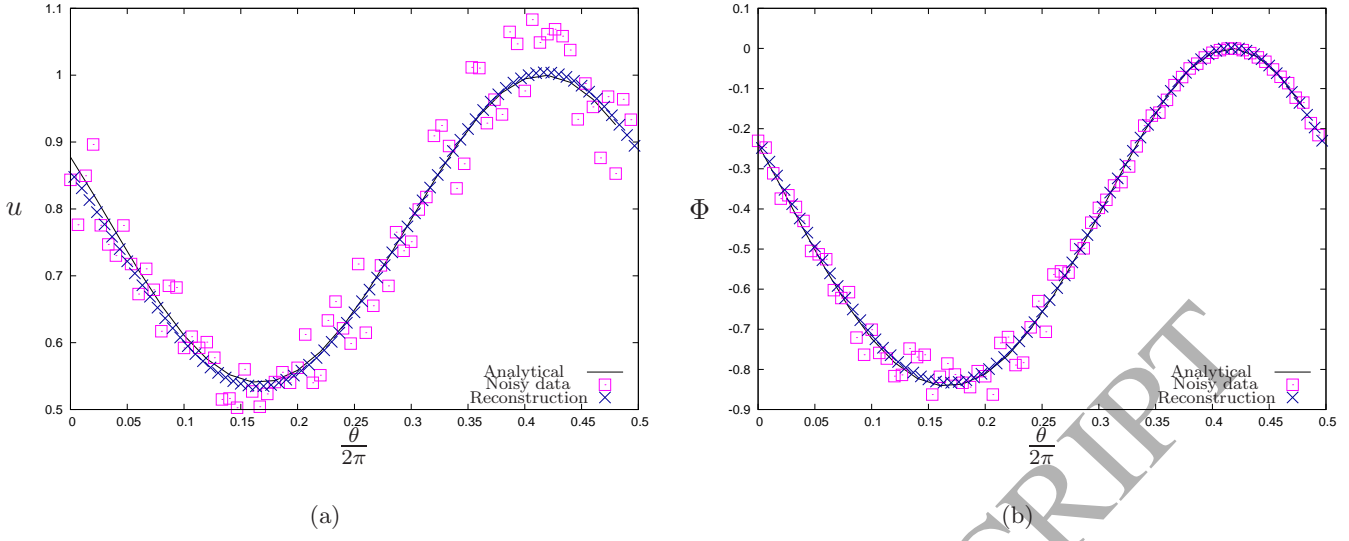


Figure 8: Reconstructions of (a) the solution,  $u$  and (b) its normal derivative  $\Phi$  on  $\Gamma_d$ , for  $c = 1.10^{-1}$  and  $\delta = 10\%$ .

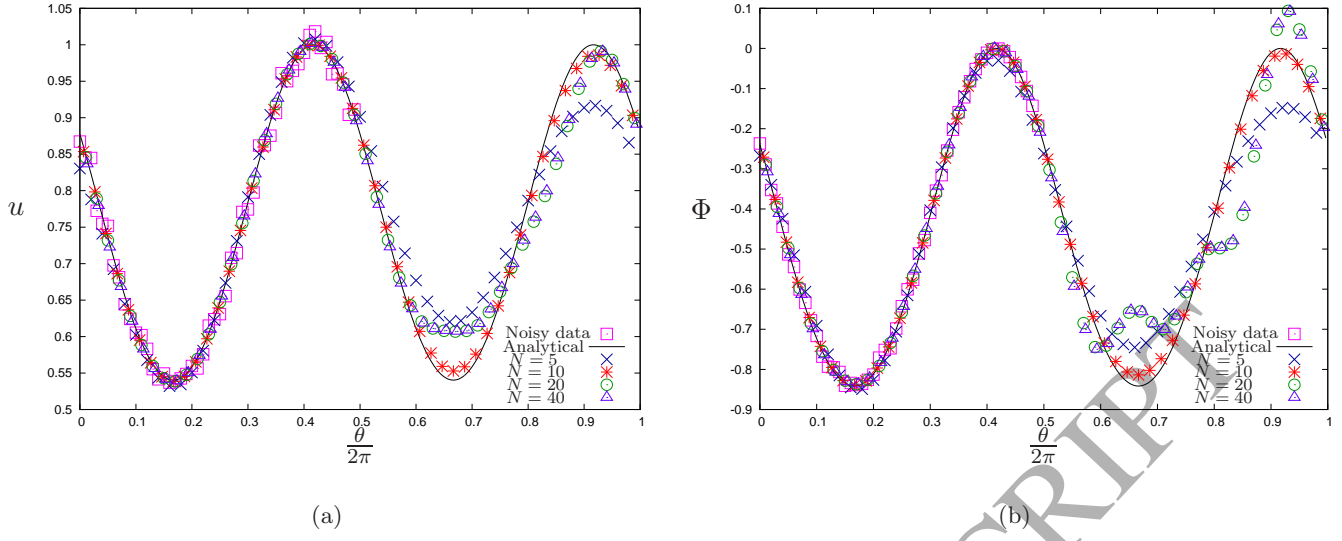


Figure 9: Influence of the number of sources,  $N$ , on the reconstructions of (a) the solution  $u$ , and (b) its normal derivative  $\Phi$  on  $\Gamma$ , for  $c = 1.10^{-1}$  and 3% noisy data.

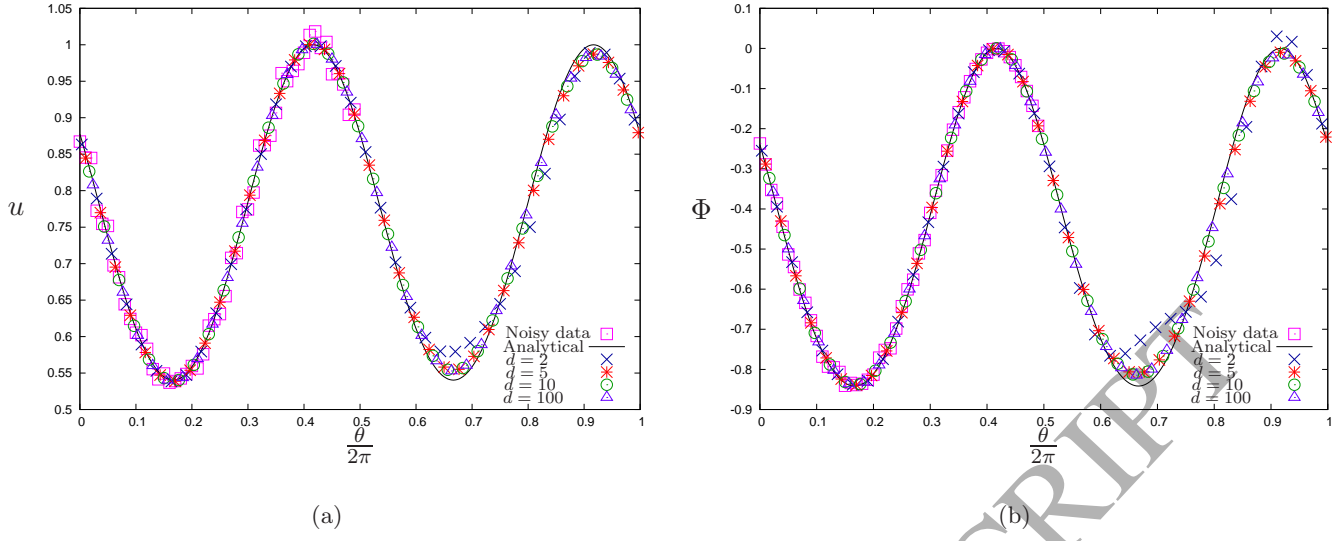


Figure 10: Influence of the distance  $d$  on the reconstruction of (a) the solution  $u$ , and (b) its normal derivative  $\Phi$  on  $\Gamma$ , for  $c = 1.10^{-1}$  and  $\delta = 3\%$ .

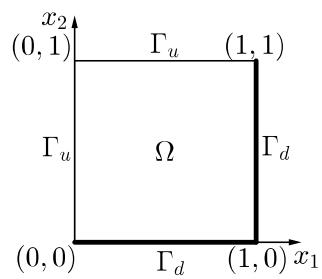


Figure 11: Schematic diagram for Example 2.

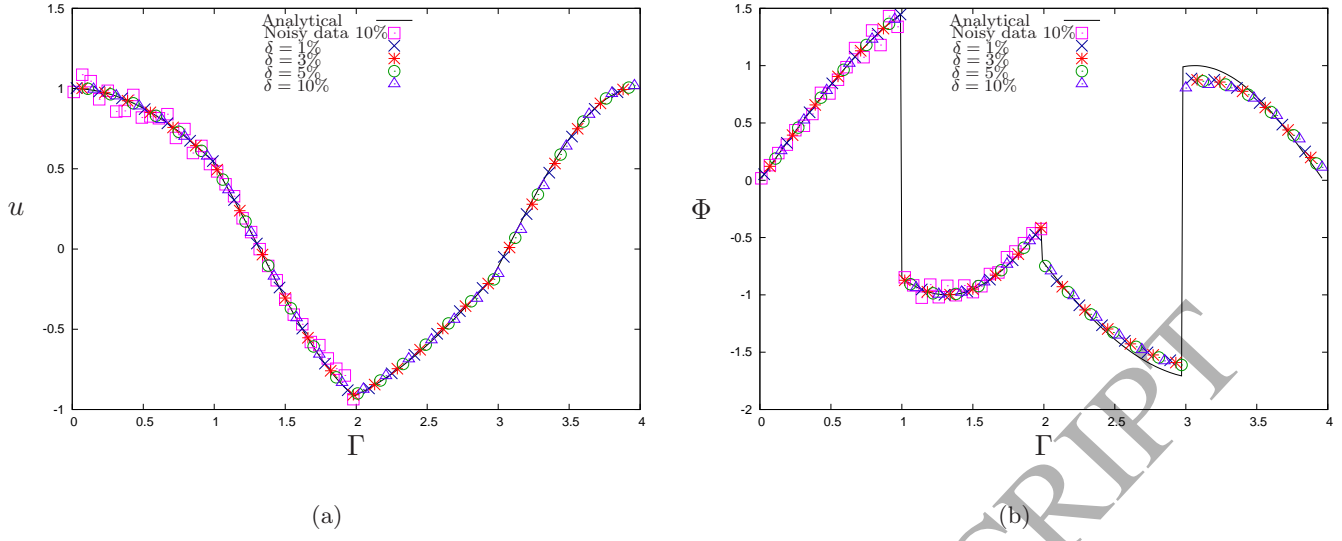


Figure 12: Reconstruction of the solution  $u$  (a), and its normal derivative  $\Phi$  (b) on  $\Gamma$ , for various levels of noise and  $c = 1$ .

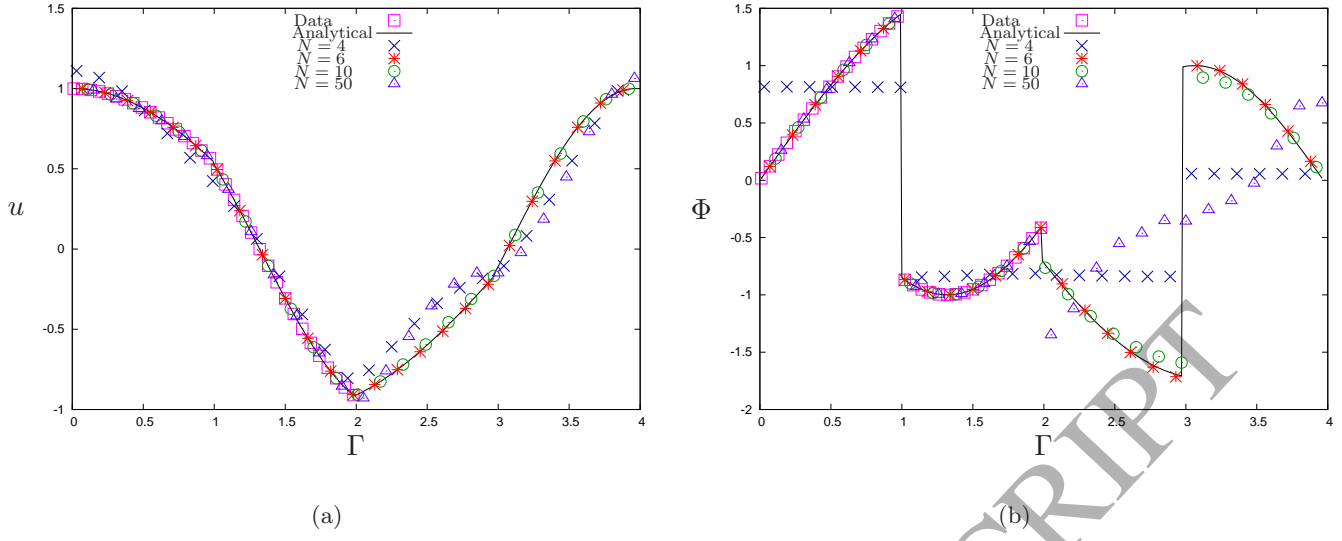


Figure 13: Influence of number of sources,  $N$ , on the reconstruction of (a) the solution  $u$ , and (b) its normal derivative  $\Phi$  on  $\Gamma$ , for  $c = 1$  and exact data.

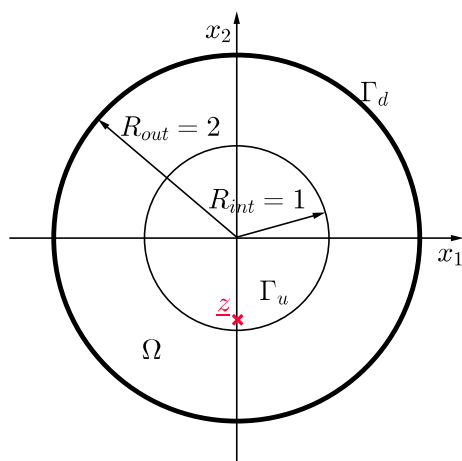


Figure 14: Skematic diagram of Example 3.

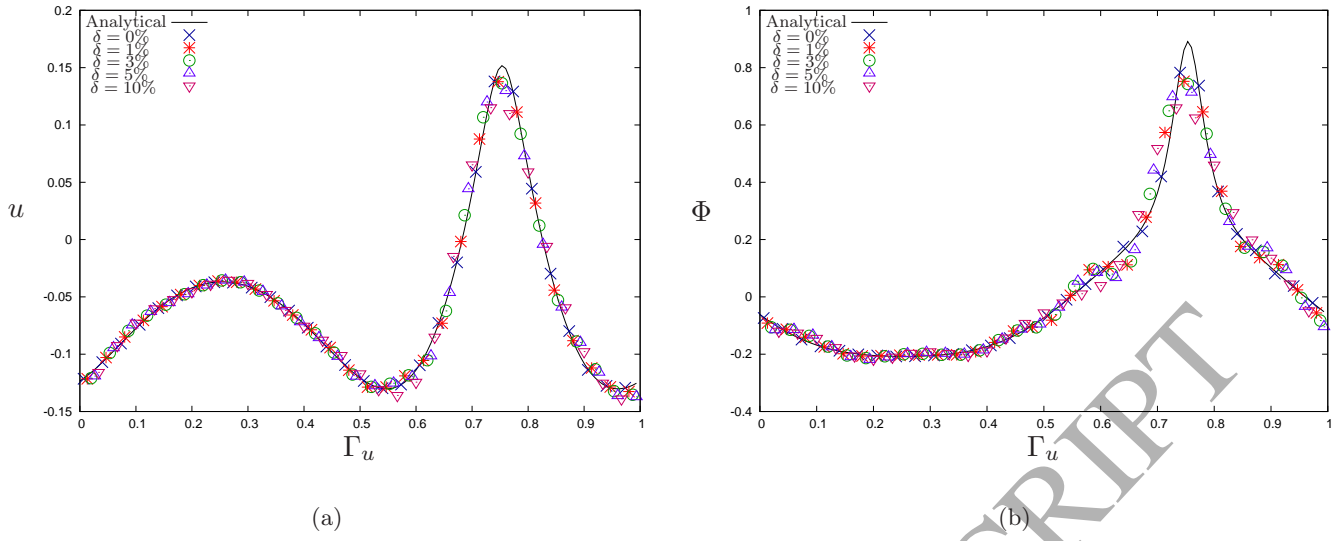


Figure 15: Reconstruction of (a) the solution  $u$ , and (b) its normal derivative  $\Phi$  on  $\Gamma_u$ , for various levels of noise.



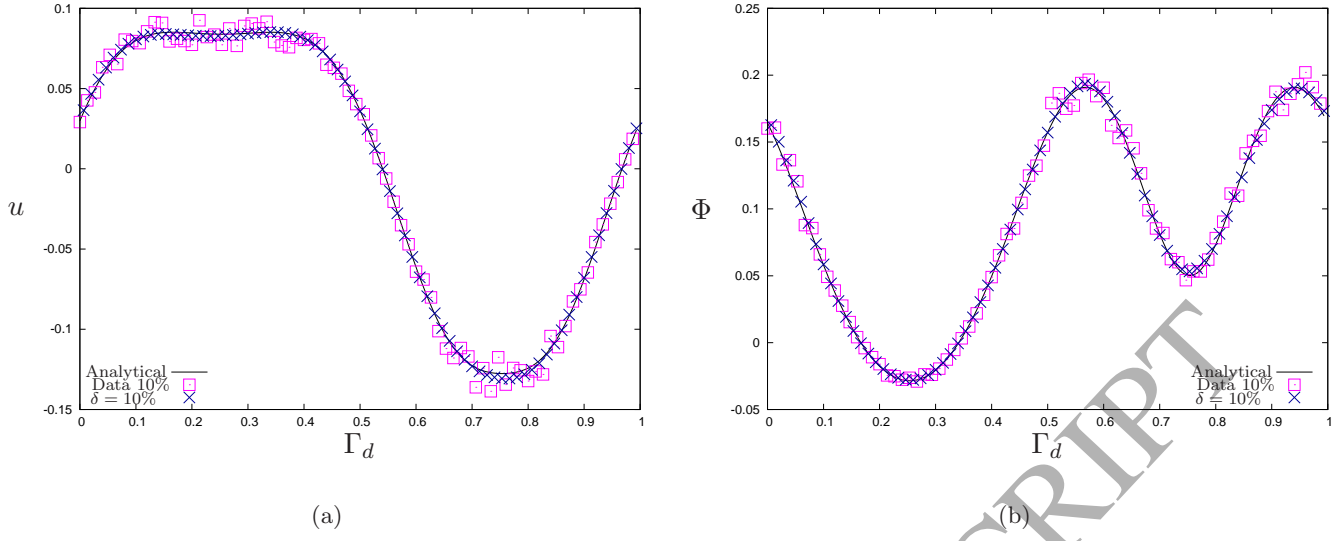


Figure 16: Reconstruction of (a) the solution  $u$ , and (b) its normal derivative  $\Phi$  on  $\Gamma_d$ , for  $\delta = 10\%$ .

| $c$         | $k$   | $\ u - u^{an}\ _{L^2(\Gamma)} / \ u^{an}\ _{L^2(\Gamma)}$ | $\ \Phi - \Phi^{an}\ _{L^2(\Gamma)} / \ \Phi^{an}\ _{L^2(\Gamma)}$ |
|-------------|-------|-----------------------------------------------------------|--------------------------------------------------------------------|
| $1.10^{-8}$ | 3     | $9.75 \times 10^{-7}$                                     | $1.10 \times 10^{-5}$                                              |
| $1.10^{-6}$ | 4     | $9.75 \times 10^{-7}$                                     | $1.10 \times 10^{-5}$                                              |
| $1.10^{-5}$ | 6     | $9.75 \times 10^{-7}$                                     | $1.10 \times 10^{-5}$                                              |
| $1.10^{-4}$ | 10    | $9.75 \times 10^{-7}$                                     | $1.10 \times 10^{-5}$                                              |
| $1.10^{-3}$ | 19    | $9.75 \times 10^{-7}$                                     | $1.10 \times 10^{-5}$                                              |
| $1.10^{-2}$ | 88    | $9.75 \times 10^{-7}$                                     | $1.10 \times 10^{-5}$                                              |
| $1.10^{-1}$ | 631   | $9.75 \times 10^{-7}$                                     | $1.10 \times 10^{-5}$                                              |
| 1           | 5265  | $9.75 \times 10^{-7}$                                     | $1.10 \times 10^{-5}$                                              |
| 10          | 38888 | $9.75 \times 10^{-7}$                                     | $1.10 \times 10^{-5}$                                              |

Table 1: Influence of the regularization parameter  $c$  on the number of iterations,  $k$ , required to achieve convergence, and the errors  $u_{error}$  and  $\Phi_{error}$

| $\delta$ | $c$         | $k$   | $\ u - u^{an}\ _{L^2(\Gamma)} / \ u^{an}\ _{L^2(\Gamma)}$ | $\ \Phi - \Phi^{an}\ _{L^2(\Gamma)} / \ \Phi^{an}\ _{L^2(\Gamma)}$ |
|----------|-------------|-------|-----------------------------------------------------------|--------------------------------------------------------------------|
| 1%       | $1.10^{-3}$ | 20    | $2.38 \times 10^{-5}$                                     | $7.41 \times 10^{-5}$                                              |
|          | $1.10^{-1}$ | 628   | $2.38 \times 10^{-5}$                                     | $7.41 \times 10^{-5}$                                              |
|          | 10          | 39088 | $2.38 \times 10^{-5}$                                     | $7.41 \times 10^{-5}$                                              |
| 3%       | $1.10^{-3}$ | 21    | $2.12 \times 10^{-4}$                                     | $6.11 \times 10^{-4}$                                              |
|          | $1.10^{-1}$ | 648   | $2.12 \times 10^{-4}$                                     | $6.11 \times 10^{-4}$                                              |
|          | 10          | 38709 | $2.12 \times 10^{-4}$                                     | $6.11 \times 10^{-4}$                                              |
| 5%       | $1.10^{-3}$ | 20    | $5.88 \times 10^{-4}$                                     | $1.69 \times 10^{-3}$                                              |
|          | $1.10^{-1}$ | 622   | $5.88 \times 10^{-4}$                                     | $1.69 \times 10^{-3}$                                              |
|          | 10          | 38751 | $5.88 \times 10^{-4}$                                     | $1.69 \times 10^{-3}$                                              |
| 10%      | $1.10^{-3}$ | 20    | $2.38 \times 10^{-3}$                                     | $6.79 \times 10^{-3}$                                              |
|          | $1.10^{-1}$ | 619   | $2.38 \times 10^{-3}$                                     | $6.79 \times 10^{-3}$                                              |
|          | 10          | 37822 | $2.38 \times 10^{-3}$                                     | $6.79 \times 10^{-3}$                                              |

Table 2: Influence of the noise level  $\delta$  and parameter  $c$  on the number of iterations,  $k$ , required to achieve convergence, and the errors  $u_{error}$  and  $\Phi_{error}$

| $N$ | $k$ | $\ u - u^{an}\ _{L^2(\Gamma)} / \ u^{an}\ _{L^2(\Gamma)}$ | $\ \Phi - \Phi^{an}\ _{L^2(\Gamma)} / \ \Phi^{an}\ _{L^2(\Gamma)}$ |
|-----|-----|-----------------------------------------------------------|--------------------------------------------------------------------|
| 5   | 47  | $7.46 \times 10^{-3}$                                     | $4.18 \times 10^{-2}$                                              |
| 10  | 648 | $2.12 \times 10^{-4}$                                     | $6.11 \times 10^{-4}$                                              |
| 20  | 128 | $1.51 \times 10^{-3}$                                     | $2.34 \times 10^{-2}$                                              |
| 40  | 139 | $1.51 \times 10^{-3}$                                     | $2.36 \times 10^{-2}$                                              |
| 80  | 148 | $1.50 \times 10^{-3}$                                     | $2.34 \times 10^{-2}$                                              |
| 150 | 462 | $7.68 \times 10^{-4}$                                     | $1.11 \times 10^{-2}$                                              |
| 300 | 242 | $1.07 \times 10^{-3}$                                     | $1.49 \times 10^{-2}$                                              |

Table 3: Influence of the number of sources,  $N$ , on the number of iterations,  $k$ , required to achieve convergence, and the errors  $u_{error}$  and  $\Phi_{error}$

| $d$ | $k$   | $\ u - u^{an}\ _{L^2(\Gamma)} / \ u^{an}\ _{L^2(\Gamma)}$ | $\ \Phi - \Phi^{an}\ _{L^2(\Gamma)} / \ \Phi^{an}\ _{L^2(\Gamma)}$ |
|-----|-------|-----------------------------------------------------------|--------------------------------------------------------------------|
| 1.5 | 35185 | $3.76 \times 10^{-2}$                                     | $9.11 \times 10^{-1}$                                              |
| 2   | 3405  | $6.32 \times 10^{-4}$                                     | $8.29 \times 10^{-3}$                                              |
| 4   | 842   | $2.32 \times 10^{-4}$                                     | $8.54 \times 10^{-3}$                                              |
| 5   | 727   | $2.21 \times 10^{-4}$                                     | $7.23 \times 10^{-4}$                                              |
| 8   | 660   | $2.13 \times 10^{-4}$                                     | $6.27 \times 10^{-4}$                                              |
| 10  | 648   | $2.12 \times 10^{-4}$                                     | $6.11 \times 10^{-4}$                                              |
| 40  | 629   | $2.09 \times 10^{-4}$                                     | $5.85 \times 10^{-4}$                                              |
| 100 | 623   | $2.09 \times 10^{-4}$                                     | $5.83 \times 10^{-4}$                                              |
| 150 | 628   | $2.09 \times 10^{-4}$                                     | $5.83 \times 10^{-4}$                                              |

Table 4: Influence of the distance,  $d$ , on the number of iterations,  $k$ , to achieve convergence, and the errors  $u_{error}$  and  $\Phi_{error}$ , for  $\delta = 3\%$  and  $c = 1.10^{-1}$

| $\delta$ | $k$   | $\ u - u^{an}\ _{L^2(\Gamma)} / \ u^{an}\ _{L^2(\Gamma)}$ | $\ \Phi - \Phi^{an}\ _{L^2(\Gamma)} / \ \Phi^{an}\ _{L^2(\Gamma)}$ |
|----------|-------|-----------------------------------------------------------|--------------------------------------------------------------------|
| 1%       | 13998 | $1.27 \times 10^{-4}$                                     | $2.10 \times 10^{-3}$                                              |
| 3%       | 13667 | $3.48 \times 10^{-4}$                                     | $2.47 \times 10^{-3}$                                              |
| 5%       | 13728 | $7.84 \times 10^{-4}$                                     | $3.01 \times 10^{-3}$                                              |
| 10%      | 13694 | $2.81 \times 10^{-3}$                                     | $5.17 \times 10^{-3}$                                              |

Table 5: Influence of the noise level,  $\delta$ , on the number of iterations,  $k$ , required to achieve convergence, and the errors  $u_{error}$  and  $\Phi_{error}$ , for  $c = 1$